An analysis of model proton-coupled electron transfer reactions via the mixed quantum-classical Liouville approach

Cite as: J. Chem. Phys. **141**, 044122 (2014); https://doi.org/10.1063/1.4890915
Submitted: 01 May 2014 . Accepted: 11 July 2014 . Published Online: 28 July 2014

Farnaz A. Shakib, and Gabriel Hanna

An analysis of model proton-coupled electron transfer reactions via the mixed quantum-classical Liouville approach

Farnaz A. Shakib and Gabriel Hanna[a)]
Department of Chemistry, University of Alberta, Edmonton, Alberta AB T6G 2G2, Canada

(Received 1 May 2014; accepted 11 July 2014; published online 28 July 2014)

The nonadiabatic dynamics of model proton-coupled electron transfer (PCET) reactions is investigated for the first time using a surface-hopping algorithm based on the solution of the mixed quantum-classical Liouville equation (QCLE). This method provides a rigorous treatment of quantum coherence/decoherence effects in the dynamics of mixed quantum-classical systems, which is lacking in the molecular dynamics with quantum transitions surface-hopping approach commonly used for simulating PCET reactions. Within this approach, the protonic and electronic coordinates are treated quantum mechanically and the solvent coordinate evolves classically on both single adiabatic surfaces and on coherently coupled pairs of adiabatic surfaces. Both concerted and sequential PCET reactions are studied in detail under various subsystem-bath coupling conditions and insights into the dynamical principles underlying PCET reactions are gained. Notably, an examination of the trajectories reveals that the system spends the majority of its time on the average of two coherently coupled adiabatic surfaces, during which a phase enters into the calculation of an observable. In general, the results of this paper demonstrate the applicability of QCLE-based surface-hopping dynamics to the study of PCET and emphasize the importance of mean surface evolution and decoherence effects in the calculation of PCET rate constants. © *2014 AIP Publishing LLC*. [http://dx.doi.org/10.1063/1.4890915]

I. INTRODUCTION

Many chemical and biological processes involve coupling between the transfer of electrons and protons.[1–4] This phenomenon, known as proton-coupled electron transfer (PCET), is at the heart of energy conversion reactions in photosynthesis and respiration.[5] Both the splitting of water to produce oxygen by the oxygen evolving complex in photosystem II[6] and the reduction of oxygen to water by cytochrome *c* oxidase in aerobic respiration,[7] involve multiple PCET steps. Due to their involvement in such vital processes, it is not surprising that PCET reactions have been the subject of intense theoretical[3,8–14] and experimental[4,14–20] research over the past two decades.

A deep understanding of the mechanisms of PCET reactions is complicated by both the quantum mechanical nature of the transferring protons and electrons and the size and complexity of the environments in which they occur. Ideally, a full quantum dynamical treatment should be used to study these reactions, but the large number of degrees of freedom (DOF) in the environments render such a treatment impossible. To circumvent this problem, simplified models of complex systems may be studied to gain qualitative insights into the PCET mechanisms and/or mixed quantum-classical schemes, which treat the transferring protons and electrons quantum mechanically and the environmental DOF classically, may be used to gain quantitative information about PCET reaction rates.

Another theoretical challenge in the study of PCET reactions is related to the different timescales of motions encountered in these systems. One may assume that a double adiabatic approximation is valid since the electronic motion is faster than the protonic motion, which is faster than the environmental motions. However, such an adiabatic assumption often fails for PCET reactions since, in many cases, neither the electrons respond instantaneously to the protonic and environmental motions nor the protons to the environmental motions.[21–23] Thus, an accurate description of PCET rates and mechanisms requires that all nonadiabatic couplings are taken into consideration.

The molecular dynamics with quantum transitions (MDQT) technique[24] is one of the most widely used mixed quantum-classical methods for simulating the nonadiabatic dynamics of quantum processes in condensed phase systems. This method was applied to PCET for the first time on a simple model containing three coupled DOF, which represent a proton, an electron, and a solvent mode.[25] The proton and electron were treated quantum mechanically, while the solvent mode was treated classically. By varying the model parameters, the authors investigated the nonadiabatic dynamics of both sequential (viz., ET followed by PT and PT followed by ET) and concerted PCET mechanisms. In a subsequent study,[26] several different methods for incorporating decoherence into MDQT (which, on its own, evolves the wave function coherently) were applied to a similar model exhibiting a large number of avoided curve crossings. It was found that the agreement between the MDQT and exact quantum results for the adiabatic state populations was excellent at very short times (up to 19 fs), but at longer times, the results begin to differ and remain significantly different for the duration of the time (i.e., 168 fs). This deviation is most likely due to an improper treatment of decoherence.

a)gabriel.hanna@ualberta.ca

In spite of the widespread application of the MDQT approach, it suffers from decoherence problems. Recently, it has been shown that MDQT does not reproduce the correct scaling for Marcus' golden rule electron transfer rate[27] and fails to generate the correct long time dynamics in the spin-boson model in strongly nonadiabatic, biased, and strong system-bath coupling regimes.[28] Several schemes have been developed in attempts to resolve these problems, but due to the fact that MDQT lacks a rigorous derivation they simply provide *ad hoc* corrections.[29,30] Therefore, in this paper, we employ for the first time a surface-hopping algorithm based on the numerical solution of the quantum-classical Liouville equation (QCLE)[31–42] to study PCET, since the QCLE inherently and rigorously accounts for quantum coherence/decoherence effects in mixed quantum-classical systems. In the QCLE-based surface-hopping approach, the classical DOF are evolved either on single adiabatic surfaces or on the mean of two adiabatic surfaces corresponding to two coherently coupled states,[40,41] as opposed to just on single adiabatic surfaces as in MDQT. For the Azzouz-Borgis model of a proton transfer reaction in a phenol trimethylamine complex dissolved in CH_3Cl,[43] it was found that the QCLE method gives a proton transfer rate constant that is approximately twice as large[44] as that given by MDQT,[45] thereby highlighting the differences between the two approaches for treating condensed phase charge transfer reactions. Hence, the QCLE approach is expected to yield more accurate rate constants for condensed phase PCET reactions and may also shed new light on their underlying mechanisms.

Since this work constitutes the first application of the QCLE approach to PCET, we chose to study the same model as in Refs. 25, 26, and 46 (based on a charge transfer model developed in Ref. 47) to (1) demonstrate the applicability of this method to PCET reactions, (2) compare and contrast, wherever possible, with the results of the standard MDQT approach in Ref. 25, and (3) investigate the role played by mean surface evolution in the concerted and sequential mechanisms for a range of subsystem-bath couplings. The paper is organized as follows: Sec. II summarizes the QCLE-based surface-hopping approach for generating nonadiabatic quantum-classical dynamics. The three PCET models studied in this work and the simulation details are presented in Secs. III and IV, respectively. Section V presents and discusses the results for these models and concluding remarks are made in Sec. VI.

II. ADIABATIC REPRESENTATION OF QUANTUM-CLASSICAL LIOUVILLE DYNAMICS

We consider a quantum subsystem that is coupled to a classical environment, whose Hamiltonian is given by

$$\begin{aligned}\hat{H}(Q,P) &= \frac{P^2}{2M} + V_e(Q) + \frac{\hat{p}^2}{2m} + \hat{V}_s(\hat{q}) + \hat{V}_c(\hat{q},Q)\\ &\equiv H_e(Q,P) + \hat{h}_s(\hat{q},\hat{p}) + \hat{V}_c(\hat{q},Q)\\ &\equiv H_e(Q,P) + \hat{h}(Q),\end{aligned} \tag{1}$$

where m, $\hat{q}$, and $\hat{p}$ are the vectors of masses, positions, and momenta of the n quantum DOF, respectively; M, Q, and P are the vectors of masses, positions, and momenta of the N classical DOF, respectively; $H_e = \frac{P^2}{2M} + V_e$ and $\hat{h}_s = \frac{\hat{p}^2}{2m} + \hat{V}_s$ are the environment and subsystem Hamiltonians, respectively; $\hat{V}_c$ is the subsystem-environment coupling potential energy, and $\hat{h} = \hat{h}_s + \hat{V}_c$ [throughout this paper, operators are capped (e.g., $\hat{A}$)]. The state of this mixed quantum-classical system can be represented in terms of the partial Wigner transform[48] of the density operator, $\hat{\rho}$, over the environmental DOF as

$$\hat{\rho}_W(X,t) = \left(\frac{1}{2\pi\hbar}\right)^N \int dZ e^{iP\cdot Z/\hbar} \langle Q - Z/2|\hat{\rho}(t)|Q + Z/2\rangle, \tag{2}$$

where $X = (Q, P)$. When $m/M \ll 1$, the dynamics of $\hat{\rho}_W(X,t)$ can be accurately described using the quantum-classical Liouville equation (QCLE)[36,49]

$$\begin{aligned}\frac{\partial}{\partial t}\hat{\rho}_W(X,t) = &-\frac{i}{\hbar}[\hat{H}_W(X,t), \hat{\rho}_W(X,t)]\\ &+\frac{1}{2}(\{\hat{H}_W(X,t), \hat{\rho}_W(X,t)\}\\ &-\{\hat{\rho}_W(X,t), \hat{H}_W(X,t)\}),\end{aligned} \tag{3}$$

where $[\cdots]$ is the commutator and the Poisson bracket $\{\cdots\}$ is defined as

$$\begin{aligned}&\{\hat{A}_W(X,t), \hat{B}_W(X,t)\}\\ &\quad= \hat{A}_W(X,t)(\overleftarrow{\nabla}_P\overrightarrow{\nabla}_Q - \overleftarrow{\nabla}_Q\overrightarrow{\nabla}_P)\hat{B}_W(X,t).\end{aligned} \tag{4}$$

Here, $\overrightarrow{\nabla}_{Q/P}$ and $\overleftarrow{\nabla}_{Q/P}$ are gradient operators with respect to Q/P which act on the term to the right and left of them, respectively.

The quantum subsystem may be represented in terms of an adiabatic basis, $|\alpha;Q\rangle$, which are the solutions of $\hat{h}(Q)|\alpha;Q\rangle = E_\alpha(Q)|\alpha;Q\rangle$. In this representation, the QCLE is given by[36]

$$\frac{\partial\rho_W^{\alpha\alpha'}(X,t)}{\partial t} = -i\sum_{\beta\beta'}\mathcal{L}_{\alpha\alpha',\beta\beta'}\rho_W^{\beta\beta'}(X,t), \tag{5}$$

where the evolution operator is defined as

$$i\mathcal{L}_{\alpha\alpha',\beta\beta'} \equiv (i\omega_{\alpha\alpha'} + iL_{\alpha\alpha'})\delta_{\alpha\beta}\delta_{\alpha'\beta'} - \mathcal{J}_{\alpha\alpha',\beta\beta'}. \tag{6}$$

In the above equation, the classical Liouville operator, $iL_{\alpha\alpha'}$, is given by

$$iL_{\alpha\alpha'} = \frac{P}{M}\cdot\frac{\partial}{\partial Q} + \frac{1}{2}\left(F_W^\alpha + F_W^{\alpha'}\right)\cdot\frac{\partial}{\partial P}. \tag{7}$$

When the quantum state indices are equal (i.e., $\alpha = \alpha'$), the classical evolution is carried out subject to the Hellmann-Feynman forces, $F_W^\alpha = -\langle\alpha;Q|\frac{\partial\hat{V}_c(\hat{q},Q)}{\partial Q}|\alpha;Q\rangle$, on a single adiabatic surface $E_\alpha(Q)$. However, when the quantum state indices are different (i.e., $\alpha \neq \alpha'$), the classical evolution is carried out on the mean of two adiabatic surfaces, $[E_\alpha(Q) + E_{\alpha'}(Q)]/2$, accompanied by quantum phase oscillations of

frequency $\omega_{\alpha\alpha'} = (E_\alpha - E_{\alpha'})/\hbar$. The term

$$\mathcal{J}_{\alpha\alpha',\beta\beta'}(t) = -\frac{P}{M}\cdot d_{\alpha\beta}\left(1+\frac{1}{2}S_{\alpha\beta}\cdot\frac{\partial}{\partial P}\right)\delta_{\alpha'\beta'} - \frac{P}{M}\cdot d^*_{\alpha'\beta'}\left(1+\frac{1}{2}S^*_{\alpha'\beta'}\cdot\frac{\partial}{\partial P}\right)\delta_{\alpha\beta} \quad (8)$$

gives rise to nonadiabatic transitions and the associated changes in the bath momentum to conserve energy. The term $S_{\alpha\beta}$ is defined as $S_{\alpha\beta} = F^\alpha_W\delta_{\alpha\beta} - F^{\alpha\beta}_W(\frac{P}{M}\cdot d_{\alpha\beta})^{-1} = E_{\alpha\beta}d_{\alpha\beta}(\frac{P}{M}\cdot d_{\alpha\beta})^{-1}$, where $d_{\alpha\beta} = \langle\alpha;Q|\frac{\partial}{\partial Q}|\beta;Q\rangle$ is the nonadiabatic coupling matrix element and $F^{\alpha\beta}_W$ is the off-diagonal matrix element of the force.

Formally, the solution of the QCLE for $\rho^{\alpha\alpha'}_W(X,t)$ can be written as

$$\rho^{\alpha\alpha'}_W(X,t) = \sum_{\beta\beta'}(e^{-i\hat{\mathcal{L}}t})_{\alpha\alpha',\beta\beta'}\rho^{\beta\beta'}_W(X)\,. \quad (9)$$

A numerical solution may be obtained using the sequential short-time propagation (SSTP) algorithm,[40] which is based on a decomposition of the propagator into short-time segments. Dividing the time interval t into S segments such that the jth segment has length $\Delta t_j = t_j - t_{j-1} = \Delta t$ (where Δt is the time step), gives

$$\rho^{\alpha_0\alpha'_0}_W(X,t) = \sum_{(\alpha_1\alpha'_1)\ldots(\alpha_S\alpha'_S)}\left[\prod_{j=1}^{S}(e^{-i\hat{\mathcal{L}}\Delta t_j})_{\alpha_{j-1}\alpha'_{j-1},\alpha_j\alpha'_j}\right]\rho^{\alpha_S\alpha'_S}_W(X), \quad (10)$$

where the short-time propagator is approximated by

$$(e^{-i\hat{\mathcal{L}}\Delta t_j})_{\alpha_{j-1}\alpha'_{j-1},\alpha_j\alpha'_j} \approx \mathcal{W}_{\alpha_{j-1}\alpha'_{j-1}}(t_{j-1},t_j)e^{-iL_{\alpha_{j-1}\alpha'_{j-1}}\Delta t_j} \times(\delta_{\alpha_{j-1}\alpha_j}\delta_{\alpha'_{j-1}\alpha'_j} + \Delta t\,\mathcal{J}_{\alpha_{j-1}\alpha'_{j-1},\alpha_j\alpha'_j}) \quad (11)$$

and $\mathcal{W}_{\alpha_{j-1}\alpha'_{j-1}}(t_{j-1},t_j) = e^{-i\omega_{\alpha_{j-1}\alpha'_{j-1}}\Delta t_j}$ is the phase factor for that segment. In the SSTP algorithm, Monte Carlo sampling is used to evaluate the multi-dimensional sums over quantum indices in Eq. (10). A typical surface-hopping trajectory generated by this algorithm is composed of segments in which the classical DOF evolve on a single adiabatic surface (when $\alpha_j = \alpha'_j$) and on the mean of two surfaces (when $\alpha_j \neq \alpha'_j$), as governed by the first term in Eq. (11). These segments are interrupted by nonadiabatic transitions, as governed by the second term in Eq. (11), which cause the classical DOF to hop to a new surface (or mean surface), followed by evolution on this surface. The details for propagating a system starting from an initial condition $\{X,\alpha_0,\alpha'_0\}$ via the SSTP algorithm are provided in Refs. 40 and 41.

III. PCET MODEL

We provide a brief outline of the model of the condensed phase PCET reaction studied herein (a more detailed description is available in Ref. 25). The PCET reaction occurs between two positively charged ions, referred to as the donor (D) and acceptor (A), which are separated by a fixed distance d_{DA}. The coordinates of the proton and electron, denoted by q_p and q_e, respectively, are measured relative to D (see Fig. 1). The coordinate of the collective solvent mode to which the proton and electron are coupled, is denoted by Q. Within our approach, the proton and electron are treated quantum mechanically, whereas the solvent mode is treated classically. The Hamiltonian of this mixed quantum-classical system is given by

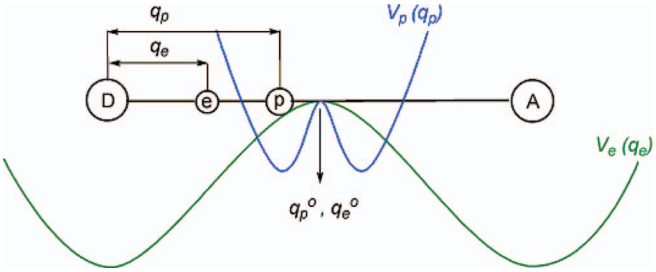

FIG. 1. Schematic representation of the one-dimensional PCET model studied in this paper. The protonic and electronic potentials (V_p and V_e, respectively) are superimposed onto the donor(D)−acceptor(A) axis. The protonic and electronic coordinates (q_p and q_e, respectively) are defined relative to the donor.

$$\begin{aligned}\hat{H} &= \hat{K}_p + \hat{K}_e + K_s + \hat{V}_p(q_p) + \hat{V}_e(q_e) + \hat{V}_{pe}(q_p,q_e) \\ &\quad + \hat{V}_{pes}(q_p,q_e,Q) + V_s(Q) \\ &\equiv \hat{h} + K_s. \end{aligned} \quad (12)$$

Here, $\hat{K}_p$ and $\hat{K}_e$ denote the kinetic energy operators of the proton and electron, respectively, K_s is the kinetic energy of the solvent mode, and $\hat{h} = \hat{H} - K_s$. The protonic potential energy operator, $\hat{V}_p$, is given by

$$\hat{V}_p(q_p) = \frac{12\Delta E}{(a_2-a_1)^3(2a_3-a_1-a_2)}\left[\frac{q_p^4}{4} - (a_1+a_2+a_3)\frac{q_p^3}{3} + (a_1a_2+a_1a_3+a_2a_3)\frac{q_p^2}{2} - (a_1a_2a_3)q_p + \frac{a_2^2\left(a_2^2-2a_2(a_1+a_3)+6a_1a_3\right)}{12}\right], \quad (13)$$

where a_1 and a_3 correspond to the positions of the two minima in this double well potential and a_2 to the position of the maximum between them. ΔE is the energy difference between the minimum at a_1 and the maximum. The electronic potential energy operator, $\hat{V}_e$, corresponding to the Coulombic interactions between the electron and the donor and acceptor charges, is given by

$$\hat{V}_e(q_e) = -\frac{C_eC_D\mathrm{erf}(q_{eD}/\xi_{eD})}{q_{eD}} - \frac{C_eC_A\mathrm{erf}(q_{eA}/\xi_{eA})}{q_{eA}}, \quad (14)$$

where C_e, C_D, and C_A are the partial charges of the electron, donor, and acceptor, respectively, and q_{eD} and q_{eA} are the distances between the electron and the donor and acceptor, respectively. In this work, both ξ_{eD} and ξ_{eA} are chosen to be equal to 1. The potential energy operator corresponding to the Coulombic interaction between the proton and electron

TABLE I. Parameters values (in atomic units) for the concerted PCET (top), sequential PT-ET (middle), and ET-PT (bottom) reactions.

$m_s = 22\,000.0$	$Q_o = 0.0$	$\omega_s = 3.72 \times 10^{-4}$	
$a_1 = 2.5$	$a_2 = 3.0$	$a_3 = 3.5$	$\Delta E = 1.2 \times 10^{-2}$
$d_{DA} = 6.0$	$C_D = 0.6$	$C_A = 0.6$	
$C_p = 0.32$	$C_e = 0.32$	$q_p^o = 3.0$	$q_e^o = 3.0$
$Q_p^o = 0.0$	$Q_e^o = 0.0$	$C_{sp} = 2.0 \times 10^{-3}$	$C_{se} = 2.0 \times 10^{-3}$
$m_s = 22\,000.0$	$Q_o = -0.4$	$\omega_s = 4.0 \times 10^{-4}$	
$a_1 = 3.5$	$a_2 = 4.0$	$a_3 = 4.55$	$\Delta E = 1.2 \times 10^{-2}$
$d_{DA} = 8.0$	$C_D = 0.6$	$C_A = 0.6$	
$C_p = 0.15$	$C_e = 0.15$	$q_p^o = 4.0$	$q_e^o = 4.0$
$Q_p^o = -0.6$	$Q_e^o = 0.0$	$C_{sp} = 1.0 \times 10^{-2}$	$C_{se} = 2.0 \times 10^{-3}$
$m_s = 22\,000.0$	$Q_o = -0.3$	$\omega_s = 4.0 \times 10^{-4}$	
$a_1 = 3.5$	$a_2 = 4.0$	$a_3 = 4.5$	$\Delta E = 1.2 \times 10^{-2}$
$d_{DA} = 8.0$	$C_D = 0.55$	$C_A = 0.55$	
$C_p = 0.15$	$C_e = 0.15$	$q_p^o = 4.0$	$q_e^o = 4.0$
$Q_p^o = 0.0$	$Q_e^o = -0.6$	$C_{sp} = 3.0 \times 10^{-2}$	$C_{se} = 4.0 \times 10^{-3}$

is given by

$$\hat{V}_{pe}(q_p, q_e) = -\frac{C_p C_e \mathrm{erf}(q_{pe}/\xi_{pe})}{q_{pe}}, \tag{15}$$

where $q_{pe} = |q_p - q_e|$ is the distance between the proton and electron. The coupling between the solvent coordinate and the proton and electron is bilinear in form[50] and is given by the following operator:

$$\hat{V}_{pes}(q_p, q_e, Q) = -C_{sp}(Q - Q_p^o)(q_p - q_p^o) - C_{se}(Q - Q_e^o)(q_e - q_e^o), \tag{16}$$

where C_{sp} and C_{se} are the coupling parameters of the proton and electron to the solvent, respectively, and Q_p^o, Q_e^o, q_p^o, and q_e^o are free parameters. When $Q < Q_{p/e}^o$ and $q < q_{p/e}^o$, the proton/electron is stabilized near the donor. Conversely, if $Q > Q_{p/e}^o$ and $q > q_{p/e}^o$, the proton/electron is stabilized near the acceptor. Finally, the dynamics of the classical solvent mode is governed by a harmonic potential of the form

$$V_s(Q) = \frac{1}{2} m_s \omega_s^2 (Q - Q_o)^2, \tag{17}$$

where m_s and ω_s are the mass and frequency, respectively, of the collective solvent mode.

By varying the parameters in the Hamiltonian, one can generate systems in which the proton and electron transfer takes place in a concerted fashion and systems in which the transfer is sequential, i.e., PT before ET (i.e., PT-ET) and vice versa (i.e., ET-PT). The parameter values used to investigate the concerted, sequential PT-ET, and sequential ET-PT mechanisms are presented in Table I. The main differences between the three sets of parameter values are as follows: The partial charges on the proton and electron are chosen to be higher (i.e., ±0.32) in the concerted case than in the sequential cases (i.e., ±0.15) since the attraction between the proton and electron should be higher for them to transfer together. In order for the proton and electron to transfer in a concerted fashion, they should also be similarly coupled to the solvent and therefore their respective couplings are chosen to be equal (i.e., $C_{sp} = C_{se}$). In contrast, in the case of sequential transfer, the proton and electron should experience different degrees of coupling to the solvent. In addition to the differences in the couplings to the solvent, the parameters Q_p^o, Q_e^o, and Q_o are different for each mechanism. Namely, $Q_p^o = Q_e^o = Q_o$ in the case of concerted PCET, $Q_p^o < Q_o$ and $Q_e^o > Q_o$ for PT-ET, and $Q_e^o < Q_o$ and $Q_p^o > Q_o$ for ET-PT. In all cases, the midpoint of the donor−acceptor distance coincides with the barrier tops of the protonic and electronic potentials (i.e., $q_p^o = q_e^o = d_{DA}/2$). The validity of these parameters can be confirmed by examining the 2D potential energy surfaces (as a function of q_p and q_e) in Figs. 3, 6, and 9 of Ref. 25.

IV. SIMULATION DETAILS

To carry out the SSTP algorithm, one needs to solve the time-independent Schrödinger equation at each step of the simulation

$$\hat{h}|\alpha; Q\rangle = E_\alpha(Q)|\alpha; Q\rangle, \tag{18}$$

where $\hat{h}$ is the model Hamiltonian given in Eq. (12). This involves expanding the adiabatic wave function $|\alpha; Q\rangle$ in an orthonormal set of two-particle basis functions as

$$|\alpha; Q\rangle = \sum_{m,n} c_{mn}^\alpha |\phi_{p(m)}\rangle |\phi_{e(n)}\rangle, \tag{19}$$

where $|\phi_{p(m)}\rangle$ and $|\phi_{e(n)}\rangle$ are one-particle basis functions and are chosen to be the solutions of the quantum harmonic oscillator for a proton and an electron, respectively, i.e.,

$$\phi_{p(m)}(q_p) = \langle q_p|\phi_{p(m)}\rangle = (2^m m!\sqrt{\pi})^{-1/2} \alpha_p^{1/2} e^{-\alpha_p^2 (q_p - q_p^o)/2} H_m(\alpha_p(q_p - q_p^o)), \tag{20}$$

and

$$\phi_{e(n)}(q_e) = \langle q_e|\phi_{e(n)}\rangle = (2^n n!\sqrt{\pi})^{-1/2} \alpha_e^{1/2} e^{-\alpha_e^2 (q_e - q_e^o)/2} H_n(\alpha_e(q_e - q_e^o)), \tag{21}$$

where m and n are integers and $H_m(q)$ is a Hermite polynomial. For convergence, we used a total of 625 two-particle basis functions in the expansion of Eq. (19), i.e., $0 < \{m, n\} < 24$. The one-particle protonic and electronic functions are centred at q_p^o and q_e^o, respectively, and $\alpha_p = 3.97$ Å^{-1} and $\alpha_e = 0.32$ Å^{-1}. We solve the eigenvalue problem, $hc = cE$, at each molecular dynamics step to obtain $\{c_{mn}^\alpha\}$ and $\{E_\alpha\}$, where h is the 625 × 625 Hamiltonian with matrix elements $h_{\{ij\}\{kl\}} = \langle \phi_{p(i)}\phi_{e(j)}|\hat{h}(Q)|\phi_{p(k)}\phi_{e(l)}\rangle$. The matrix elements $h_{\{ij\}\{kl\}}$ are calculated using the trapezoid rule with 100 points evenly spaced over the range $q_p = 1.06/1.59$ Å to $q_p = 2.12/2.65$ Å for the protonic integrals in the case of the concerted/sequential mechanisms and 700 points over the range $q_e = -3.17$ Å to $q_e = 6.35$ Å for the electronic integrals in the case of all mechanisms.

The nonadiabatic coupling matrix element, $d_{\alpha\beta}$, for this model is given by

$$d_{\alpha\beta} = \frac{-1}{\Delta E_{\alpha\beta}} \langle \alpha; Q | \frac{\partial \hat{h}}{\partial Q} | \beta; Q \rangle$$
$$= \frac{1}{\Delta E_{\alpha\beta}} \sum_{mnkl} c^{\alpha}_{mn} c^{\beta}_{kl} [C_{sp} \langle \phi_{p(m)} | (q_p - q^o_p) | \phi_{p(k)} \rangle \delta_{nl}$$
$$+ C_{se} \langle \phi_{e(n)} | (q_e - q^o_e) | \phi_{e(l)} \rangle \delta_{mk}], \quad (22)$$

and the Hellmann-Feynman forces, F^{α}_{W}, are given by

$$F^{\alpha}_{W} = -\langle \alpha; Q | \frac{\partial \hat{h}(Q)}{\partial Q} | \alpha; Q \rangle$$
$$= \sum_{mnkl} c^{\alpha}_{mn} c^{\alpha}_{kl} [C_{sp} \langle \phi_{p(m)} | (q_p - q^o_p) | \phi_{p(k)} \rangle \delta_{nl}$$
$$+ C_{se} \langle \phi_{e(n)} | (q_e - q^o_e) | \phi_{e(l)} \rangle \delta_{mk}]. \quad (23)$$

After summing the Hellmann-Feynman forces and the classical forces, the classical DOF are propagated using the velocity-Verlet algorithm with a time step of 2.4 fs.

V. RESULTS

A. Adiabatic potential energy surfaces and nonadiabatic couplings

The ground (1,1) and first-excited (2,2) state adiabatic potential energy surfaces (and the corresponding mean surfaces [(1,2) or (2,1)]) as a function of the solvent coordinate for the concerted, sequential PT-ET, and sequential ET-PT mechanisms are shown in Fig. 2. In this work, the dynamics is restricted to the two lowest states since, according to Ref. 25, the higher excited states are rarely populated for the range of initial momenta considered.[51] For concerted PCET (top panel of Fig. 2), both the ground and first excited state surfaces are symmetric about $Q = 0$ Å. The minimum energy gap of 0.44 kcal/mol between the surfaces occurs at the barrier top of the ground state surface (i.e., at $Q = 0$ Å). The ground state surface exhibits two minima, one at $Q = -0.4$ Å and the other at $Q = 0.4$ Å, corresponding to stable solvent configurations in which the proton and electron are near the donor and acceptor, respectively. This is confirmed by examining the ground state adiabatic wave function, which can be found in Fig. 4 of Ref. 25. In contrast, the excited state surface exhibits a single minimum at $Q = 0.0$ Å. An examination of the excited-state wave functions (not shown) reveals that for $Q < 0$ Å, the proton and electron are near the acceptor, while for $Q > 0$ Å they are near the donor. The mean surface exhibits a shallow well, whose minimum occurs at $Q = 0.0$ Å. In the concerted case, a PCET reaction takes place when the system starts at the donor site on the ground-state surface (i.e., at $Q < 0.21$ Å) and moves to the acceptor site on the ground-state surface (i.e., at $Q > 0.21$ Å).

In the case of sequential PCET, the ground and first-excited state surfaces are asymmetric about the ground-state barrier tops (see Fig. 2 for close-ups on the barrier top regions and Fig. 1 of the supplementary material[52] for the full surfaces). For PT-ET, the ground state surface has a barrier top centered at $Q = -0.46$ Å, the excited state surface exhibits

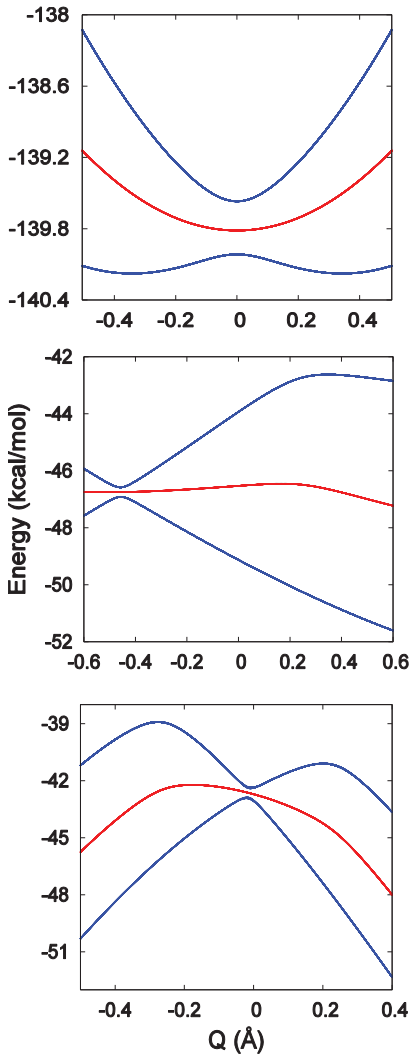

FIG. 2. Adiabatic potential energy surfaces as a function of the solvent coordinate, Q, for the concerted (top), PT-ET (middle), and ET-PT (bottom) reactions. The blue curves correspond to the ground and first excited state surfaces, while the red curves correspond to the mean surfaces.

one main well (with two shallow wells flanking it), and the mean surface exhibits a relatively flat region centered at $Q = -0.46$ Å (with two shallow wells flanking it). The minimum energy gap between the ground and first excited states is 0.33 kcal/mol. For ET-PT, the ground and first-excited state surfaces are more asymmetric about the ground-state barrier top than the PT-ET surfaces, and the mean surface exhibits a broad barrier top. The minimum energy gap is 0.46 kcal/mol at $Q = -0.02$ Å. The characters of the ground and first-excited state wave functions at different solvent configurations are shown in Figs. 7 and 10 of Ref. 25. For PT-ET, the ground-state wave function reveals that at $Q = -0.5$ Å (i.e., to the left of the barrier top), both the proton and electron are near the donor, while at $Q = -0.32$ Å the proton transfers to the acceptor but the electron remains at the donor. However, at $Q = 0.11$ Å, both the proton and electron are located near the acceptor. Hence, once the proton has transferred to the acceptor, there is no barrier associated with the motion of the solvent as the electron transfers to the acceptor. For ET-PT, the situation is reversed. The ground-state wave function

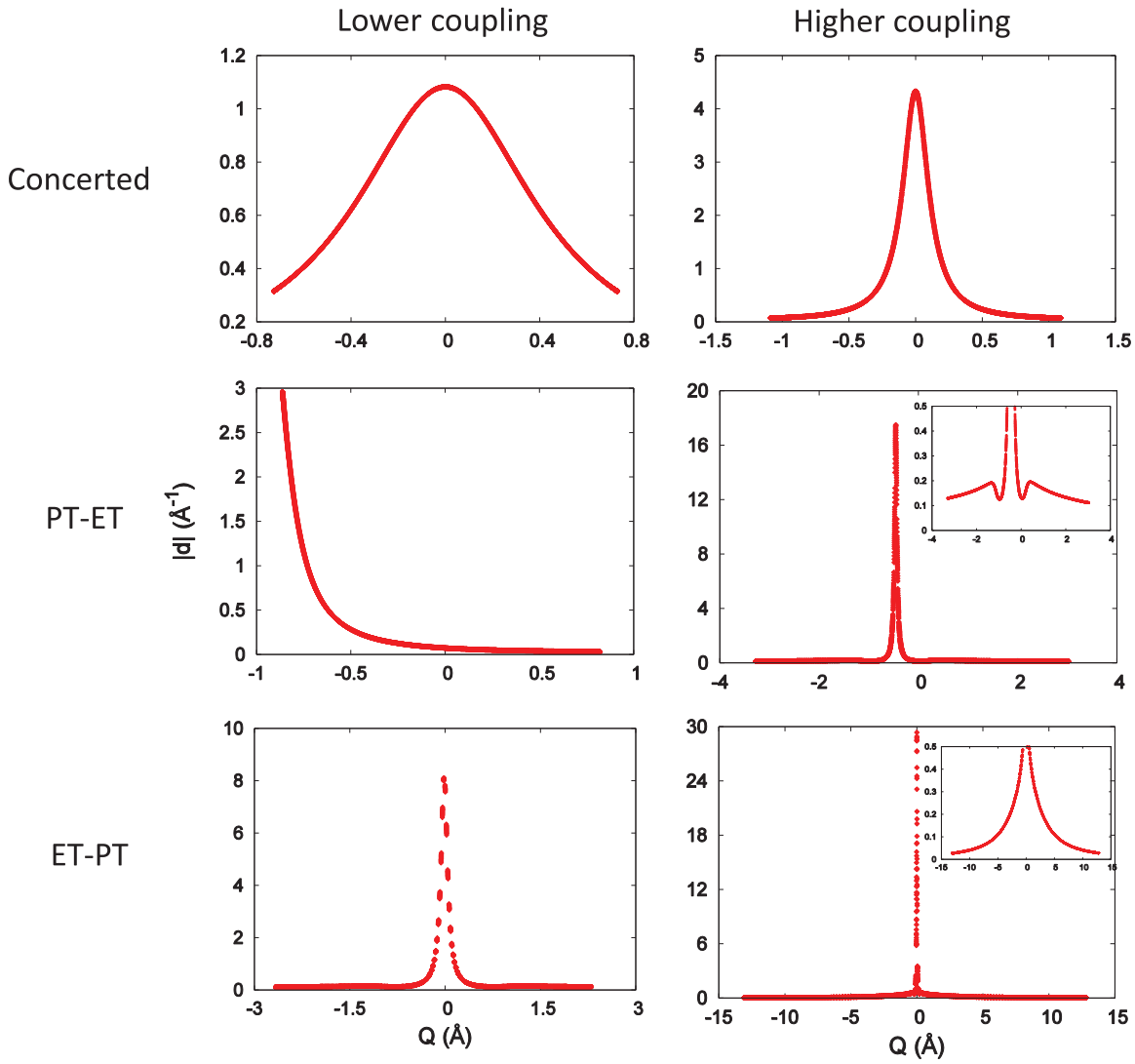

FIG. 3. Nonadiabatic coupling strength, $|d_{12}|$, as a function of the solvent coordinate, Q, computed for concerted PCET (top panels), PT-ET (middle panels), and ET-PT (bottom panels). The insets zoom in on the sections corresponding to lower $|d_{12}|$ values. (Left panels) Lower proton/electron-solvent coupling. The coupling constants for concerted PCET, PT-ET, and ET-PT are $C_{sp} = C_{se} = 5 \times 10^{-4}$, $C_{sp}/C_{se} = 2.5 \times 10^{-3}/5 \times 10^{-4}$, and $C_{sp}/C_{se} = 7.5 \times 10^{-3}/1 \times 10^{-3}$, respectively. (Right panels) Higher proton/electron-solvent coupling. The coupling constants for concerted PCET, PT-ET, and ET-PT are $C_{sp} = C_{se} = 2 \times 10^{-3}$, $C_{sp}/C_{se} = 1 \times 10^{-2}/2 \times 10^{-3}$, and $C_{sp}/C_{se} = 3 \times 10^{-2}/4 \times 10^{-3}$, respectively.

reveals that at $Q = -0.48$ Å (i.e., to the left of the barrier top), both the proton and electron are near the donor, while at $Q = -0.16$ Å (i.e., to the left of the barrier top), the electron transfers to the acceptor but the proton remains at the donor. However, at $Q = 0.16$ Å, both the proton and electron are located near the acceptor. Examination of the first-excited state wave functions for PT-ET and ET-PT reveals that at Q equal to 0.42 Å and 0.45 Å, respectively, the proton and electron are near the acceptor. Therefore, a successful reaction takes place when the system starts at the donor site on the ground-state surface (viz., at $Q < -0.6$ Å and -0.2 Å for PT-ET and ET-PT, respectively) and moves to the acceptor site on either the ground or excited state surfaces (viz., at $Q > 0.11$ Å and 0.42 Å for the ground and first-excited states, respectively, of PT-ET and $Q > 0.2$ Å and 0.4 Å for the ground and first-excited states, respectively, of ET-PT).

To gain insight into the strength of the nonadiabatic coupling between the adiabatic surfaces and, hence, into the regions where nonadiabatic transitions are likely to occur, we calculated $|d_{12}|$ as a function of the solvent configuration Q for the various PCET mechanisms. In the right-hand panels of Fig. 3, we show $|d_{12}|$ vs. Q for concerted PCET (top panel), PT-ET (middle panel), and ET-PT (bottom panel). As expected, $|d_{12}|$ is peaked at the Q values corresponding to the ground-state barrier top where the energy gap between the ground and first-excited state surfaces is the smallest. We also see that $|d_{12}|$ attains higher values in ET-PT than in PT-ET than in concerted PCET. This is a reflection of the differences in the energy gaps and relative curvatures of the ground- and first-excited state surfaces between the mechanisms. When we zoom in on the section of the PT-ET graph corresponding to lower $|d_{12}|$ values (see insets of Fig. 3), we see "bumps" on either side of the barrier top, which stretch over a relatively wide range of solvent configurations, and are due to the presence of wells on the excited-state surface (see Fig. 1 of the supplementary material[52]). Therefore, outside of the barrier

top region, one can still expect some nonadiabatic transitions to occur (albeit to a much lesser extent than in the barrier top region).

In Subsection V B, we describe the nature of the nonadiabatic dynamics observed in the concerted, sequential PT-ET, and sequential ET-PT mechanisms. In each case, we initialized trajectories with several different momenta, P_i, but with the same value of the solvent coordinate, Q_i.

B. Nonadiabatic dynamics

1. Concerted PCET

We generated an ensemble of 1000 trajectories, starting from $Q_i = -0.24$ Å on the ground state for the following values of the initial momentum: $P_i = 4.0$, 7.0, 10.0, and 15.0 a.u. Each trajectory is terminated when it reaches a donor or acceptor configuration in the reactant or product well (i.e., $|Q| > 0.21$ Å) on the ground state surface. For this ensemble of trajectories, we started by examining the percentage of trajectories, % PCET, which successfully go from the reactant well on the ground state to the product well on the ground state, whether adiabatically or nonadiabatically. The top panel of Fig. 4 illustrates % PCET as a function of the initial momentum. After an initial decrease from 100% to 71% in going from $P_i = 4.0$ a.u. to $P_i = 7.0$ a.u., % PCET remains relatively constant with increasing P_i. This should be contrasted with the results in Ref. 25, where substantial decreases in % PCET are observed with increasing P_i. This difference is due to the fact that our dynamics can occur on the mean surface, whose shallow well can facilitate the PCET. Also shown in the top panel of Fig. 4 are the percentages of the sub-ensemble of trajectories that successfully underwent PCET with 0 (i.e., adiabatic), 2, 4, 6, 8, and 10 nonadiabatic transitions. It should be noted that only even numbers of jumps were considered since successful PCETs cannot terminate on the mean surfaces. At $P_i = 4.0$ a.u., 100% of PCETs occur adiabatically, but when P_i increases to 7.0 a.u., there is a large drop in the percentage of adiabatic PCETs to 46% due to the onset of nonadiabatic transitions. For $P_i \geq 10.0$ a.u., we see that the percentages of reactive trajectories undergoing any number of jumps do not change significantly with increasing P_i, with ~50% of PCETs occurring adiabatically, ~23% nonadiabatically via two nonadiabatic transitions, and ~27% nonadiabatically via four or more nonadiabatic transitions. This means that beyond $P_i =$ 7.0 a.u., approximately 0.50% × 72% = 36% of the entire ensemble of trajectories undergo PCET adiabatically, 0.23% × 72% = 17% undergo PCET via two jumps, and 0.27% × 72% = 19% undergo PCET via four or more jumps. As can be seen, the majority of reactive, nonadiabatic trajectories follow the (1, 1) → (1, 2)/(2, 1) → (1, 1) pathway, and a smaller percentage follow the (1, 1) → (1, 2)/(2, 1) → (2, 2) → (1, 2)/(2, 1) → (1, 1) pathway.

The top panel of Fig. 5 presents the percentage of time spent on the various surfaces over the ensemble of 1000 trajectories. We see that for $P_i = 4.0$ a.u., 100% of the time is spent on the (1,1) surface. For this initial momentum, the system is unable to make any jumps. However, as P_i is increased, we see a large initial drop in the time spent on the (1,1) surface

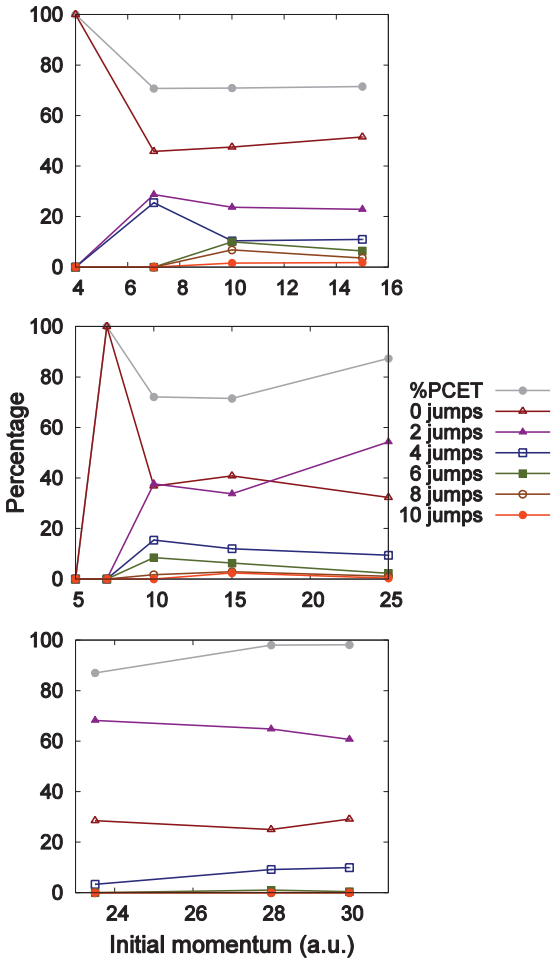

FIG. 4. Percentage of trajectories which successfully undergo a PCET reaction (denoted by % PCET) and the percentage of these trajectories which contain 0, 2, 4, 6, 8, and 10 nonadiabatic transitions (denoted by 0 jumps, 2, jumps, etc.) as a function of the initial momentum for the concerted (top), PT-ET (middle), and ET-PT (bottom) reactions.

to 19% (and eventually to 7% for $P_i = 15.0$ a.u.), an increase in the time spent on the (1,2) and (2,1) surfaces to 70%, and a gradual increase in the time spent on the (2,2) surface to 26% for $P_i = 15.0$ a.u. The increases in the (1,2)/(2,1) and (2,2) percentages take place since the system has sufficient momentum to frequently enter into the strong nonadiabatic coupling region. It should be noted that in the limit of a sufficiently large ensemble, the (1,2) and (2,1) percentages should be equal. Overall, these results underscore the importance of mean surface evolution in the ensemble.

2. Sequential PT-ET mechanism

We generated ensembles of 1000 trajectories, starting from $Q_i = -0.58$ Å on the ground state for the following values of the initial momentum: $P_i = 5.0$, 7.0, 10.0, 15.0, and 25.0 a.u. Each trajectory is terminated when it reaches an acceptor configuration on either the ground or first excited state (i.e., $Q > 0.11$ Å and $Q > 0.42$ Å, respectively) or returns to a donor configuration (i.e., $Q < -0.6$ Å) on the ground state. The value of % PCET varies from 0% to 100% to 72% to 72% to 87% in going from $P_i = 5.0$ a.u. to $P_i = 25.0$ a.u., not

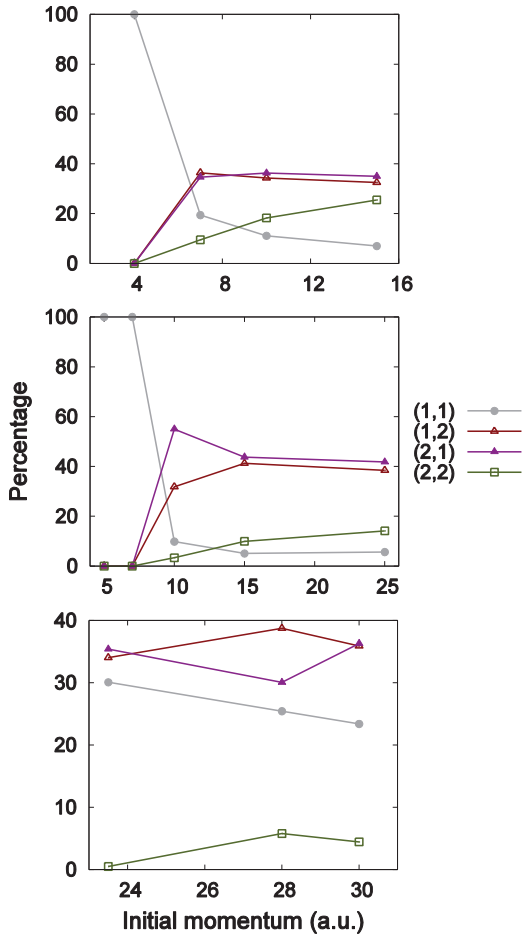

FIG. 5. Percentage of time (out of the entire ensemble) spent on the ground state (1,1), mean [(1,2) and (2,1)], and first-excited state (2,2) surfaces as a function of the initial momentum for the concerted (top), PT-ET (middle), and ET-PT (bottom) mechanisms.

exhibiting any noticeable trend beyond $P_i = 7.0$ a.u. (see middle panel of Fig. 4). The minimum momentum, i.e., $P_i = 7.0$ a.u., at which trajectories begin to undergo PCET reactions is somewhat higher than that in the concerted case, i.e., $P_i = 4.0$ a.u. This is a reflection of the longer distance between the donor and acceptor for PT-ET than for concerted PCET (see Table I), which leads to a higher ground-state barrier for PT-ET than for concerted PCET (see Fig. 2). Increasing the initial solvent momentum beyond $P_i = 15.0$ a.u. leads to a higher % PCET since the probability of nonadiabatic transitions from the (1,2)/(2,1) to the (1,1) and (2,2) surfaces becomes high enough such that more jumps to these surfaces occur outside of the barrier top region. This should be contrasted with what was found in Ref. 25, where % PCET starts at 9%, fluctuates, and ultimately reaches its maximum value (83%) at the highest P_i value of 25 a.u. In this case, the absence of mean surface evolution would prevent the possibility for % PCET to dramatically increase for the intermediate values of the initial momentum.

The middle panel of Fig. 4 shows the percentages of the sub-ensemble of trajectories that successfully underwent PCET with 0, 2, 4, 6, 8, and 10 nonadiabatic transitions. For $P_i = 10.0$ a.u., in contrast to the concerted case, we see that the percentages of 2- and 4-jump trajectories are significantly higher, viz., 38% and 15%, respectively (at the expense of 0-jump trajectories). When P_i is increased from 10.0 a.u. to 25 a.u., the percentages change, with each profile exhibiting a different behaviour. The 0-jump contribution increases to a maximum (41% at $P_i = 15$ a.u.) and then decreases; the 2-jump contribution decreases to a minimum (34% at $P_i = 15$ a.u.) and then increases dramatically; the 4- and 6-jump contributions decrease gradually (while the higher jump contributions become negligible).

The trends of the percentages of time spent on each surface are very similar to those of concerted PCET, but the magnitudes are somewhat different (see middle panel of Fig. 5). Of particular note, we see that less time is spent on the (2,2) surface and more time on the mean surfaces than in concerted PCET, for all initial momenta in common. In going from $P_i = 15.0$ a.u. to $P_i = 25.0$ a.u., we see that the percentages of time spent on the mean surfaces exhibit very slight decreases, while the percentage of time spent on the (2,2) surface increases slightly. Again, we see that evolution on the mean surfaces plays an important role in the ensemble ($\sim$80% for $P_i \geq 10.0$).

3. Sequential ET-PT mechanism

We generated ensembles of 1000 trajectories, starting from $Q_i = -0.5$ Å on the ground state for the following (relatively high) values of the initial momentum: $P_i = 23.5$, 28.0, and 30.0 a.u. Each trajectory is terminated when it reaches a donor or acceptor configuration on either the ground or excited state surface (viz., $|Q| > 0.2$ Å or $|Q| > 0.4$ Å, respectively). From the bottom panel of Fig. 4, we see that % PCET increases from 87% to 98% as P_i is increased. This is in stark contrast to what was found in Ref. 25, where % PCET ranges from 8% to 74% in going from $P_i = 23.5$ to 30.0 a.u. This difference is due to the fact that our dynamics can occur on the mean surface, whose convex shape can strongly enhance the PCET.

The bottom panel of Fig. 4 also shows the percentages of the sub-ensemble of trajectories that successfully underwent PCET with 0, 2, 4, 6, 8, and 10 nonadiabatic transitions. As P_i increases from 23.5 to 30.0 a.u., the percentages of 0- and 2-jump trajectories do not change significantly, while the percentage of 4-jump trajectories increases substantially (from 3% to 10%). In contrast to the case of PT-ET, for similarly high values of the momenta (viz., $P_i = 23.5$ a.u. of ET-PT vs. $P_i = 25.0$ a.u. of PT-ET), there is a smaller percentage of adiabatic trajectories (29% for ET-PT vs. 32% for PT-ET), a larger percentage of 2-jump trajectories (68% for ET-PT vs. 54% for PT-ET), and a smaller percentage of 4-jump trajectories (3% for ET-PT vs. 9% for PT-ET).

As in the concerted and PT-ET cases, the trajectories spend much of their time ($\sim$70%) on the (1,2) and (2,1) surfaces for all initial momenta. However, it is interesting to note that for these relatively high values of P_i, we see a substantial percentage (23%–30%) of time spent on the (1,1) surface, in contrast to the concerted and PT-ET cases. This is likely due to an increase in the percentages of 2-jump trajectories (relative to the concerted and PT-ET cases) that take the system

away from the (1,2) and (2,1) surfaces and back to the (1,1) surface.

4. Role of phase factor

A unique feature of the QCLE-based surface-hopping algorithm is the phase factor from Eq. (11), $\mathcal{W}_{\alpha_{j-1}\alpha'_{j-1}}(t_{j-1}, t_j) = e^{-i\omega_{\alpha_{j-1}\alpha'_{j-1}}\Delta t_j}$, which enters into the evolution of an observable.[40,41] Fluctuations of the classical coordinates can cause this phase factor to oscillate in time differently for each trajectory and, therefore, averaging over an ensemble of trajectories can lead to destructive interference in the expectation value of an observable. Therefore, one way to gauge the *decohering* effect of the environment on the quantum subsystem is to compute the average of the real part of $\mathcal{W}(t)$, $\langle \mathrm{Re}[\mathcal{W}(t)]\rangle$, over an ensemble of trajectories starting from a given Q_i and a distribution of momenta centred around a given P_i (corresponding to a temperature of 300 K). In Fig. 6, we see that $\langle \mathrm{Re}[\mathcal{W}(t)]\rangle$ (averaged over 1000 trajectories) exhibits a different decay time and profile for each PCET mechanism considered. In the case of concerted PCET, PT-ET, and ET-PT, $\langle \mathrm{Re}[\mathcal{W}(t)]\rangle$ decays to zero in 50–150 fs, 75–100 fs, and 75 fs, respectively. Although the initial decay rates are different for each mechanism, in general, the initial decay rate increases as P_i is increased. These results suggest that phase effects are important when studying PCET processes on ultrafast timescales, and will differ depending on the mechanism in question.

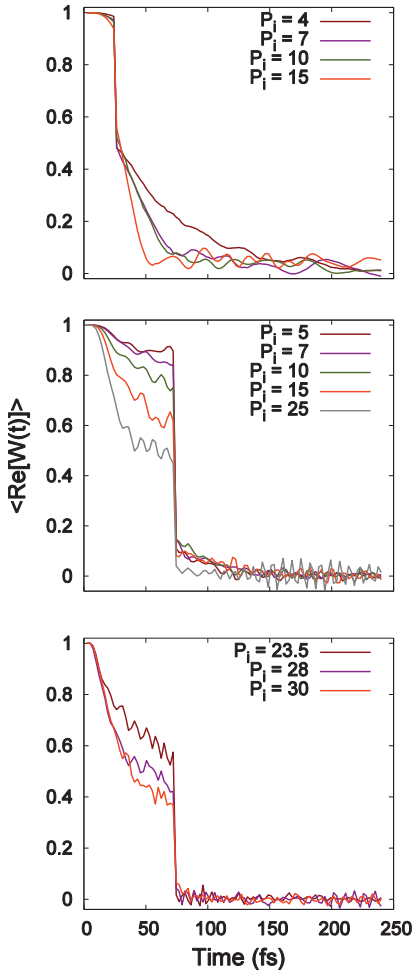

FIG. 6. Average of the real part of $\mathcal{W}(t)$, $\langle \mathrm{Re}[\mathcal{W}(t)]\rangle$, over an ensemble of trajectories starting from $Q_i = -0.24$, -0.58, and -0.5 Å and initial momentum distributions (corresponding to a temperature of 300 K) centred around different P_i, for the concerted (top), PT-ET (middle), and ET-PT (bottom) reactions, respectively.

C. Effect of proton/electron-solvent coupling strength

We investigated the effect of varying the coupling strength between the proton/electron and the solvent on the nonadiabatic coupling, $|d_{12}|$, in order to gain insight into how this will affect the nonadiabatic dynamics. The results for the original coupling strength are contrasted with those for a lower coupling strength in Fig. 3. For concerted PCET, as the coupling strength increases, we see that the overall distribution of $|d_{12}|$ values becomes narrower and grows in height. This is mainly due to the change in the relative curvatures of the ground- and excited-state surfaces. Therefore, as the coupling strength increases, the probability of nonadiabatic transitions becomes very high at the barrier top and drops off quickly outside of this region. That being said, at lower coupling strengths, the probability of nonadiabatic transitions is higher outside of the barrier top region. For PT-ET, increasing the coupling not only causes an increase in the central peak height of the distribution, but also a shift in the peak position to larger Q values. Therefore, as the coupling strength increases, the region where the probability of nonadiabatic transitions is highest shifts to larger Q values. For ET-PT, increasing the coupling also causes an increase in the central peak height. Thus, in all three cases, increasing the coupling will significantly affect the nonadiabatic dynamics, but not necessarily in the same way.

In Fig. 7, we show the effect of varying the coupling strength between the proton/electron and the solvent on % PCET (based on ensembles of 1000 trajectories) for each value of the initial momentum. For each mechanism, the seven different sets of coupling constants studied are listed in Table II in order of increasing coupling strength (note that the original ratio of C_{sp} to C_{se} is maintained for each mechanism). In the concerted case (see top panel of Fig. 7), as the coupling strength is increased for $P_i = 4.0$ and 7.0 a.u., % PCET first decreases, then increases to 100%, and, beyond a certain threshold coupling strength, drops to zero since the barrier becomes too high for reactions to occur (see Fig. 3 of the supplementary material[52]). This behaviour is likely due to the fact that for coupling strengths lower than the threshold coupling strength, trajectories traversing towards the acceptor configuration may return to the donor side via the mean surface, while at the threshold coupling strength the energy gaps are sufficiently high to inhibit nonadiabatic transitions, but the barrier is low enough to allow all of the trajectories to reach the stable acceptor configuration. For $P_i = 10.0$ a.u., % PCET decreases gradually and then suddenly drops to zero, whereas for $P_i = 15.0$ a.u., % PCET decreases gradually up to a certain intermediate coupling strength, but then increases. In this case, there is no sudden drop to zero, since for $P_i = 15.0$ a.u.

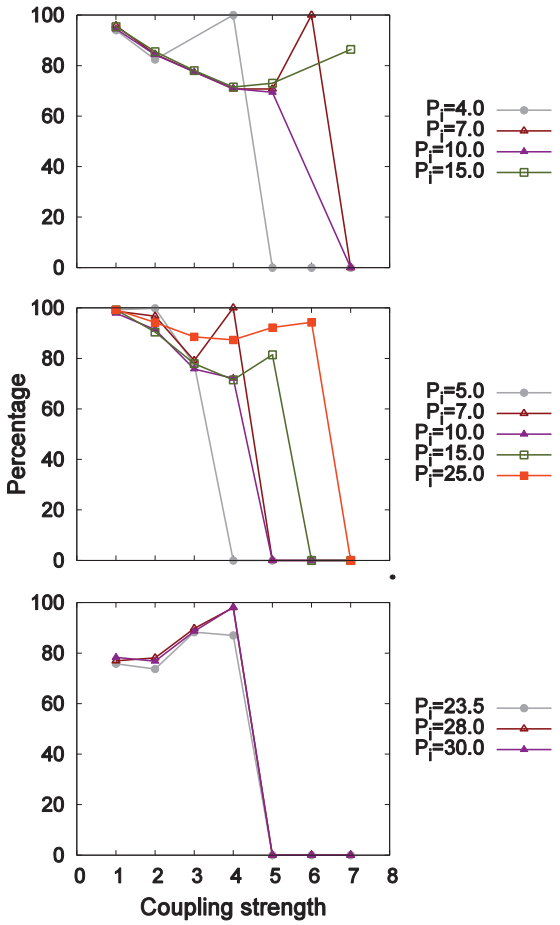

FIG. 7. Percentage of trajectories which successfully undergo a PCET reaction as a function of the coupling strength between the proton/electron and the solvent for various initial momenta, P_i, for the concerted (top), PT-ET (middle), and ET-PT (bottom) reactions. The x-axis labels, 1–7, represent seven sets of coupling constants $\{C_{sp}, C_{se}\}$ (values given in Table II), listed in order of increasing strength.

the system has sufficient kinetic energy to overcome the barrier. It should be noted that several points were omitted from the top panel of Fig. 7, since for these particular combinations of P_i and coupling strength the system gets "stuck" on the mean surface for a long time and, as a result, these trajectories could not terminate within a reasonable amount of time (for $P_i = 4.0$ a.u./strength $= 3$, 7.0 a.u./strength $= 3$, 10.0 a.u./strength $= 6$, and 15.0 a.u./strength $= 6$, 374, 733, 711, and 957 trajectories terminated, respectively). In contrast, the percentage of successful adiabatic PCETs (see top panel of Fig. 2 of the supplementary material[52]) is lower than % PCET for intermediate and high coupling strengths (except for the coupling strengths where the $P_i = 4.0$ and 7.0 a.u. percentages spike to 100% before dropping to zero). Therefore, the fact that % PCET is larger than the percentage of successful adiabatic PCETs is directly due to nonadiabatic transitions. Similar trends are observed in the case of PT-ET (see middle panel of Fig. 7). Here, we see that % PCET drops to zero for all initial momenta and the coupling strength at which the drop occurs increases with increasing initial momenta. The percentage of successful adiabatic PCETs is higher than % PCET for some low coupling strengths, but lower than % PCET for intermediate and higher coupling strengths (see middle panel of Fig. 2 of the supplementary material[52]) than in the case of % PCET. This indicates that nonadiabatic transitions can play a dual role, inhibiting PCETs under low coupling conditions and enhancing them under higher ones. In the case of ET-PT (see bottom panel of Fig. 7), % PCET increases to a maximum value at a coupling strength of 4, followed by sudden drops to zero for all initial momenta considered. In stark contrast, the magnitudes of the percentages of successful adiabatic PCETs are much lower and gradually decrease as the coupling strength is increased for all values of the initial momentum considered (see bottom panel of Fig. 2 of the supplementary material[52]). Thus, for this mechanism, these initial momenta, and these coupling strengths, nonadiabatic dynamics on the mean and excited-state surfaces leads to a dramatic change in the reaction dynamics.

The effect of varying the coupling strength between the proton/electron and the solvent on $\langle \mathrm{Re}[\mathcal{W}(t)] \rangle$ (with the average calculated in the same fashion as in Subsection V B 4) is shown in Fig. 8. In all three mechanisms, higher coupling to the solvent leads to a faster initial decay of $\langle \mathrm{Re}[\mathcal{W}(t)] \rangle$, as expected, with a faster decay occurring for concerted PCET compared to the sequential PCETs. However, the rates and profiles of the decays are mechanism-dependent. For example, under low coupling conditions, a long-lived lower-frequency oscillation in $\langle \mathrm{Re}[\mathcal{W}(t)] \rangle$ is observed in the case of concerted PCET, while short-lived high-frequency oscillations are observed in the sequential PCETs. These plots demonstrate the sensitivity of the phase factor to the solvent dynamics in the various mechanisms and, hence, emphasize the importance of including this phase factor for a

TABLE II. Seven sets of proton/electron-solvent coupling constants (i.e., $\{C_{sp}, C_{se}\}$) considered in this study for the three PCET mechanisms, ranging from low (1) to high (7) coupling. All values are in atomic units.

		Coupling constants						
		1	2	3	4	5	6	7
Concerted	C_{sp}	1×10^{-4}	5×10^{-4}	1×10^{-3}	2×10^{-3}	3×10^{-3}	4×10^{-3}	8×10^{-3}
	C_{se}	1×10^{-4}	5×10^{-4}	1×10^{-3}	2×10^{-3}	3×10^{-3}	4×10^{-3}	8×10^{-3}
PT-ET	C_{sp}	5×10^{-4}	2.5×10^{-3}	5×10^{-3}	1×10^{-2}	1.5×10^{-2}	2×10^{-2}	4×10^{-2}
	C_{se}	1×10^{-4}	5×10^{-4}	1×10^{-3}	2×10^{-3}	3×10^{-3}	4×10^{-3}	8×10^{-3}
ET-PT	C_{sp}	3.75×10^{-3}	7.5×10^{-3}	1.5×10^{-2}	3×10^{-2}	6×10^{-2}	1.2×10^{-1}	2.4×10^{-1}
	C_{se}	5×10^{-4}	1×10^{-3}	2×10^{-3}	4×10^{-3}	8×10^{-3}	1.6×10^{-2}	3.2×10^{-2}

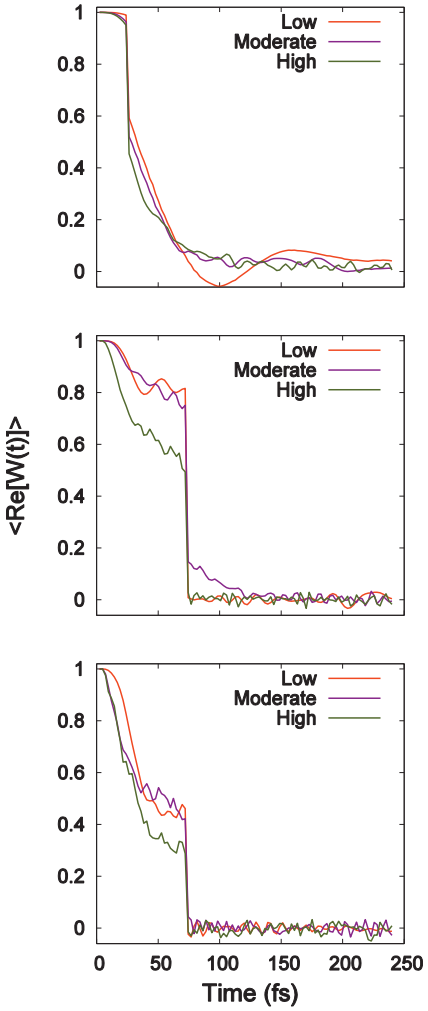

FIG. 8. Average of the real part of $\mathcal{W}(t)$, $\langle \mathrm{Re}[\mathcal{W}(t)]\rangle$, over an ensemble of trajectories starting from $Q_i = -0.24$, -0.58, and -0.5 Å and an initial momentum distribution (corresponding to a temperature of 300 K) centred around $P_i = 10$, 10, and 28 a.u. for the concerted (top), PT-ET (middle), and ET-PT (bottom) reactions, respectively, calculated for three different sets of proton/electron-solvent coupling strengths.

proper treatment of the decoherence in a wide range of ultrafast PCET reactions.

VI. CONCLUDING REMARKS

In this paper, we presented the first application of quantum-classical Liouville dynamics to the study of PCET. A minimal model of a condensed phase PCET reaction consisting of a proton, an electron, and a solvent coordinate was studied, which had been investigated previously using the MDQT method.[25] Varying the model's parameters allowed us to study both concerted and sequential PCET mechanisms under a wide range of subsystem-bath couplings. For each mechanism, we generated an ensemble of 1000 trajectories, starting from the same position of the solvent on the ground adiabatic state (corresponding to the donor configuration) but different values of the momentum, to study the effect of increasing the momentum on the nonadiabatic dynamics. Successful PCETs end in the acceptor configuration (on the ground state in the case of concerted PCET and either the ground or excited state in the case of the sequential PCETs), occurring either adiabatically on the ground state or nonadiabatically after transitions between states.

In the case of concerted PCET, as the initial momentum is increased, the percentage of successful PCET reactions displays an initial decrease but then remains relatively constant. Except for the lowest initial momentum (viz., $P_i = 4.0$ a.u.), approximately half of these PCETs occur adiabatically and the other half nonadiabatically via primarily the following pathway: (1,1)→(1,2)/(2,1)→(1,1). Interestingly, for $P_i = 7.0$ a.u., the percentage of 4-jump trajectories is higher than for any other value of the initial momentum in any mechanism. In the case of PT-ET, increasing the initial solvent momentum beyond $P_i = 15.0$ a.u. leads to a higher % PCET since more nonadiabatic transitions from the (1,2)/(2,1) to the (1,1) and (2,2) surfaces occur outside of the barrier top region. As in the case of concerted PCET, the 0- and 2-jump reactive trajectories are the two main contributors. In the case of ET-PT, increasing the initial solvent momentum over the range of high initial momenta considered leads to an increase in the percentage of successful PCET reactions (to almost 100%). It also substantially increases the percentage of 4-jump reactions, at the expense of the adiabatic and 2-jump reactions. Overall, our results for % PCET drastically differ from those in Ref. 25 due to the fact that, regardless of the mechanism, large amounts of time are spent on the mean surface for all initial momenta. This underscores the importance of including the mean surface, (α, α'), in the nonadiabatic dynamics, especially when it is significantly different in character from the (α, α) and (α', α') surfaces. While on the mean surface, the observable in question (e.g., a rate constant) acquires a phase, which can lead to either constructive or destructive interference upon averaging over an ensemble of trajectories. For each PCET mechanism considered, we observed a different decay profile for the average of the real part of the phase factor, $\langle \mathrm{Re}[\mathcal{W}(t)]\rangle$, suggesting that coherence/decoherence effects may be important when studying ultrafast PCET processes and may vary from mechanism to mechanism.

We also investigated the effects of varying the coupling strength between the proton/electron and the solvent on % PCET and on $\langle \mathrm{Re}[\mathcal{W}(t)]\rangle$ for all three mechanisms. In the case of % PCET, we found that both the weight and nature of the role played by nonadiabatic dynamics depend on the coupling strength, initial momentum, and the mechanism considered. For all mechanisms studied, % PCET suddenly drops to zero at high coupling strengths due to the emergence of high reaction barriers. In addition, in most cases, nonadiabatic transitions to the various surfaces facilitate PCETs, but in some cases they can inhibit PCETs. In the case of the phase factor, an increase in the coupling strength leads to a faster decay of $\langle \mathrm{Re}[\mathcal{W}(t)]\rangle$, with faster initial decays observed in concerted PCET than in the sequential ones. We also found that the rates and profiles of these decays are mechanism-dependent.

Given the more rigorous basis of the QCLE surface-hopping approach and the fact that it yields significantly different results than the MDQT approach for the minimal model considered in this study, the QCLE method could provide new insight into the nonadiabatic dynamics of a wide range of PCET reactions and, therefore, form the basis for future

investigations of PCET reactions in more complex systems. The next steps would involve demonstrating the use of the QCLE method for computing experimental observables such as state populations and rate constants, and investigating the role of decoherence in PCET models with more elaborate solvents.

ACKNOWLEDGMENTS

This work was supported by funding from the University of Alberta and Alberta Innovates Technology Futures.

[1]T. Meyer, M. Huynh, and H. Holden Thorp, Angew. Chem., Int. Ed. **46**, 5284 (2007).
[2]M. Huynh and T. Meyer, Chem. Rev. **107**, 5004 (2007).
[3]S. Hammes-Schiffer and A. Stuchebrukhov, Chem. Rev. **110**, 6939 (2010).
[4]D. Weinberg, C. Gagliardi, J. Hull, C. Fecenko Murphy, C. Kent, B. Westlake, A. Paul, D. Ess, D. Granville McCafferty, and T. Meyer, Chem. Rev. **112**, 4016 (2012).
[5]V. R. I. Kaila, M. I. Verkhovsky, and M. Wikstrom, Chem. Rev. **110**, 7062 (2010).
[6]B. A. Diner and F. Rappaport, Annu. Rev. Plant Biol. **53**, 551 (2002).
[7]G. T. Babcock and M. Wikstrom, Nature (London) **356**, 301 (1992).
[8]R. Cukier and D. Nocera, Annu. Rev. Phys. Chem. **49**, 337 (1998).
[9]A. Soudackov and S. Hammes-Schiffer, J. Chem. Phys. **113**, 2385 (2000).
[10]I. Rostov and S. Hammes-Schiffer, J. Chem. Phys. **115**, 285 (2001).
[11]M. Kobrak and S. Hammes-Schiffer, J. Phys. Chem. B **105**, 10435 (2001).
[12]S. Hammes-Schiffer and A. Soudackov, J. Chem. Phys. **112**, 14108 (2008).
[13]P. E. Siegbahn and M. Blomberg, Chem. Rev. **110**, 7040 (2010).
[14]H. Petek and J. Zhao, Chem. Rev. **110**, 7082 (2010).
[15]J. Warren, T. Tronic, and J. Mayer, Chem. Rev. **110**, 6961 (2010).
[16]C. Costentin, Chem. Rev. **108**, 2145 (2008).
[17]N. Song, C. J. Gagliardi, R. A. Binstead, M.-T. Zhang, H. Thorp, and T. J. Meyer, J. Am. Chem. Soc. **134**, 18538 (2012).
[18]M. M. Roubelakis, D. K. Bediako, D. K. Dogutan, and D. G. Nocera, Energy Environ. Sci. **5**, 7737 (2012).
[19]J. N. Schrauben, R. Hayoun, C. N. Valdez, M. Braten, L. Fridley, and J. M. Mayer, Science **336**, 1298 (2012).
[20]A. A. Pizano, J. L. Yang, and D. G. Nocera, Chem. Sci. **3**, 2457 (2012).
[21]A. Soudackov and S. Hammes-Schiffer, J. Chem. Phys. **111**, 4672 (1999).
[22]Y. Georgievskii and A. A. Stuchebrukhov, J. Chem. Phys. **113**, 10438 (2000).
[23]S. Hammes-Schiffer, J. Phys. Chem. Lett. **2**, 1410 (2011).
[24]J. Tully and R. Preston, J. Chem. Phys. **93**, 1061 (1990).
[25]J.-Y. Fang and S. Hammes-Schiffer, J. Chem. Phys. **106**, 8442 (1997).
[26]J.-Y. Fang and S. Hammes-Schiffer, J. Chem. Phys. **107**, 8933 (1997).
[27]B. R. Landry and J. E. Subotnik, J. Chem. Phys. **135**, 191101 (2011).
[28]A. Kelly and T. Markland, J. Chem. Phys. **139**, 014104 (2013).
[29]M. J. Bedard-Hearn, R. E. Larsen, and B. J. Schwartz, J. Chem. Phys. **123**, 234106 (2005).
[30]B. R. Landry and J. E. Subotnik, J. Chem. Phys. **137**, 22A513 (2012).
[31]C. C. Martens and J. Fang, J. Chem. Phys. **106**, 4918 (1997).
[32]A. Donoso and C. C. Martens, J. Chem. Phys. **102**, 4291 (1998).
[33]A. Donoso and C. C. Martens, J. Chem. Phys. **112**, 3980 (2000).
[34]A. Donoso, D. Kohen, and C. C. Martens, J. Chem. Phys. **112**, 7345 (2000).
[35]M. Santer, U. Manthe, and G. Stock, J. Chem. Phys. **114**, 2001 (2001).
[36]R. Kapral and G. Ciccotti, J. Chem. Phys. **110**, 8919 (1999).
[37]S. Nielsen, R. Kapral, and G. Ciccotti, J. Stat. Phys. **101**, 225 (2000).
[38]C. Wan and J. Schofield, J. Chem. Phys. **113**, 7047 (2000).
[39]C. Wan and J. Schofield, J. Chem. Phys. **112**, 4447 (2000).
[40]D. MacKernan, R. Kapral, and G. Ciccotti, J. Phys.: Condens. Matter **14**, 9069 (2002).
[41]G. Hanna and R. Kapral, J. Chem. Phys. **122**, 244505 (2005).
[42]D. MacKernan, G. Ciccotti, and R. Kapral, J. Phys. Chem. B **112**, 424 (2008).
[43]H. Azzouz and D. Borgis, J. Chem. Phys. **98**, 7361 (1993).
[44]G. Hanna and R. Kapral, J. Chem. Phys. **128**, 164520 (2008).
[45]S. Hammes-Schiffer and J. Tully, J. Chem. Phys. **101**, 4657 (1994).
[46]J.-Y. Fang and S. Hammes-Schiffer, J. Chem. Phys. **107**, 5727 (1997).
[47]S. Shin and H. Metiu, J. Chem. Phys. **102**, 9285 (1995).
[48]E. Wigner, Phys. Rev. **40**, 749 (1932).
[49]R. Kapral, Annu. Rev. Phys. Chem. **57**, 129 (2006).
[50]For subsystem-bath coupling potentials that are linear in the bath coordinate, MQCL dynamics is exact. The only approximation made in the sequential short-time propagation solution of the MQCL equation is the momentum jump approximation, which has been shown numerous times to be a very good approximation.
[51]The authors of Ref. 25 arrived at this conclusion on the basis of simulations involving 100 trajectories per initial momentum.
[52]See supplementary material at http://dx.doi.org/10.1063/1.4890915 for figures.